

An e-ANOVA Tuned $d-q$ Controller for Single Stage Grid Interface SPV system with Power Quality Improvement

P. Meganathan*[‡], C. Sasi**, P. Pugazhendiran***, P. Nammalvar****

*Department of Electrical and Electronics Engineering, Sri Venkateshwaraa College of Engineering and Technology, Ariyur, Puducherry India – 605102

**Department of Electrical, FEAT, Annamalai University, Chidambaram, Tamilnadu, India – 608002

***Department of Electrical and Electronics Engineering, IFET College of Engineering, Villupuram, Tamilnadu, India – 605108

****Department of Electrical and Electronics Engineering, Krishnasamy College of Engineering and Technology, Cuddalore, Tamilnadu, India – 607109

(megaisagem@gmail.com, saasi_eeee@yahoo.co.in, pugazhendiran@gmail.com, alvar1976@gmail.com)

[‡]Corresponding Author: Mr. P. Meganathan, Assistant Professor/EEE, Sri Venkateshwaraa College of Engineering and Technology, Ariyur, Puducherry India – 605102, Tel: +91 8870984192, megaisagem@gmail.com

Received: 30.10.2021 Accepted: 22.11.2021

Abstract- In yesteryears, statistical models were popular due to their quantitative outcomes. This paper uses Analysis of Variance (ANOVA) techniques to tune Proportional-Integral (PI) in the $d-q$ controller of Voltage Source Inverter (VSI) of a single-stage three-phase grid integrated Solar Photovoltaic (SPV) systems. The control approach of VSI is interfaced to three-phase grid integrated SPV systems at fast varying irradiance and compensates the non-linear load tied at Point of Common Coupling (PCC). This control scheme provides smooth operation of load balancing and harmonics reduction in grid performance. The enhanced ANOVA (e-ANOVA) tuned $d-q$ controller has the advantage of better perfection than conventional methods, decreases the training data time, reduces the size of the input sample, and retains the sample discretionary information. The substantiated proposed controller is performed under steady-state and dynamic conditions. The proposed controller is compared with conventional $d-q$ controller result shows better response time, satisfactory behavior in uniform and variable irradiance. Simulation illustration shows the ability to improve grid power stability with less fluctuation and Total Harmonic Distortion (THDs). The grid performance and its THDs of voltages and currents are attained within the limitation of harmonic content imposed by international standards. The simulation of the SPV system is carried out in MATLAB/Simulink and their results are validated.

Keywords Analysis of Variance, ANOVA, Photovoltaic, Single-Stage Inverter, Power quality.

1. Introduction

An expansion of electrical generation is necessary due to the industries and population growth. The magnification of greenhouse gas emission and depletion of fossil fuel gives way for non-conventional energy sources to meet out the electrical demands. An echoing of non-conventional energy is solar photovoltaic (SPV) systems in view of feasible solar

energy, in skipping fuel cost, easy maintenance, unpolluted and silent generation. The SPV generation was popularly applied in solar water heating and pumping system, solar electric vehicles, solar power plants, space satellites, etc. [1]. The SPV panels are connected in series and parallel combinations of solar cells in order to generate SPV power [2, 3, 4]. The SPV system yields power from photovoltaic arrays which depend on varying environmental conditions,

temperature, and solar irradiance. The characteristics of SPV power are non-linear curves with fluctuation. For better SPV power, maximum power point (MPP) is needed, and locating of MPP is known as maximum power point tracking (MPPT). These day's researchers are intended to utilize a vast number of MPPT methods for tracing the MPP of the SPV system under fast varying atmosphere conditions.

The traditional MPPT techniques are Perturb and Observe (P&O), Incremental Conductance (IC), current sweep, and constant voltage methods [5]. In addition, robotic soft computing constructs several MPPT techniques like Genetic Algorithm (GA), Slide Mode Control (SMC), Ant Colony Optimization (ACO), Artificial Neural Network (ANN), Particle Swarm Optimization (PSO), Fuzzy Logic Controller (FLC), etc. In [6] had explained the various MPPT techniques and their issues for enhancing the SPV system's efficiency. In [7] had presented the multi-variable P&O algorithms for control signals in a fast varying atmospheric condition which reduces the voltage burden in DC/DC converter. In [8] intended an improved IC technique for achieving MPPT and removes the oscillation at greater efficiency.

In [9] had implemented modified particle velocity-based PSO (MPV-PSO) algorithm for tracing MPP with small variation in array voltage and it ensures eminent tracking efficiency. Whereas [10] proposes a novel overall distribution PSO (OD-PSO) algorithm for improving the accuracy of MPPT in SPV systems. In [11] had implemented self-tuning fuzzy with PI controller to derive the control signal for MPP and its output voltage are attained by a boost converter. While in [12] fuzzy-based algorithm is intended to ensure the improvement in the voltage gain of a boost converter. These SPV systems are classified as standalone systems or grid-connected systems. The standalone photovoltaic system operates independently of the electric grid which operates during sunlight hours with and without the battery storage systems [13]. The grid-connected systems are connected parallel to electric grids. It is divided into three-phase single-stage grid integrated and three-phase double-stage grid integrated [14, 15, 16].

Out of these, grid integration the inverter and its control strategies become part of SPV systems. The choice of inverter and its control strategies is a part of vital role in grid synchronization with pure sinusoidal injection. For grid integration systems widely used inverter is Current Source Inverter (CSI), Voltage Source Inverter (VSI) and Multilevel Inverter (MLI). Various optimal control strategies have been discussed by researchers, and the most commonly used control strategies are linear controllers, non-linear controllers, predictive controllers [17], robust controllers, adaptive controllers, and intelligent controllers. However, in [18] the conventional controller PSO-PI-based controller is inferior to the PPA-based controller for grid-connected systems and its performances are compared with spider graphs and boxplot analysis. In [19] the grid-connected inverters are compared with HERIC, H5, and H6. The inverter output voltage is calculated by proposed Chrip Z-transformation (CZT) spectrum analysis FFT which is more efficient than FFT analysis. In [20] proposed the three-level

active neutral point clamped (ANPC) inverter to decrease the common-mode (CM) noise in undetermined parasitic capacitance of SPV panels. In [21] the conventional CSI is compared with improved CSI by intending a novel low voltage ride through (LVRT) for the period of sag in grid voltage. The intended CSI solves the badly behaved property by way of adding chopper circuits to the grid-connected inverters. In [22] FLC-based control strategies are presented in grid-connected inverters to minimize the harmonics, switching losses, and power factor.

In this research work, a three-phase single-stage grid integrated SPV system is considered. For conversion of DC-AC, VSI is employed in the SPV system for grid power integration and its function in the $d-q$ current control method [23]. Along with Analysis of Variances (ANOVA) tuned PI controller, the $d-q$ control strategies improve the grid stability with less fluctuation and decrease the total harmonic distortions (THDs). The performance of the SPV system using e-ANOVA tuned $d-q$ controller technique is tested under the fast varying atmospheric conditions and the results are validated in a steady-state, dynamic state, and grid performance by MATLAB/Simulink environment.

In this work, Section 2 discusses modelling and its description of the SPV system chosen in simulation work. An implementation e-ANOVA tuning PI in $d-q$ control strategies in VSI is represented in Section 3. Section 4, presents the configuration of the SPV system and its operations. The performances of SPV for the proposed system are illustrated with simulation results in Section 5. In the end, a conclusion describes the fulfilment of research work.

2. Modelling and its Equivalent Circuit of SPV System

The equivalent circuit of the SPV cell is shown in Fig. 1 where the current source is connected in anti-parallel to a diode that sets up PN junction. Moreover, the outcomes of SPV cells are controlled by solar irradiance and nearby temperature [24]. The mathematical equation of the SPV cell is given by equation (1)

$$I_{PV} = I_{ph} - I_d - I_{sh} \tag{1}$$

$$\text{but, } I_d = I_s e^{\left(\left(\frac{V_{PV} + I_{PV} R_s}{nV_m} \right) - 1 \right)} \tag{2}$$

$$\text{and } I_{sh} = \left(\frac{V_{PV} + I_{PV} R_s}{R_{sh}} \right) \tag{3}$$

Substituting (2) and (3) in equation (1) we get

$$I_{PV} = I_{ph} - I_s e^{\left(\left(\frac{V_{PV} + I_{PV} R_s}{nV_m} \right) - 1 \right)} - \left(\frac{V_{PV} + I_{PV} R_s}{R_{sh}} \right) \tag{4}$$

Where, V_{PV} - Output voltage of the PV cell (V), V_m - Thermal voltage (V), I_{PV} - Generated PV current (A), I_{ph} - Cell photocurrent (A), I_d - Current through a parallel diode (A), I_{sh} - Current through a shunt resistance (A), I_s - Diode reverse saturation current (A), R_s - Lumped series resistance (Ω), R_{sh}

- Lumped shunt resistance (Ω), G - Irradiance (W/m^2), n - Quality factor of the diode which is between 1 and 2.

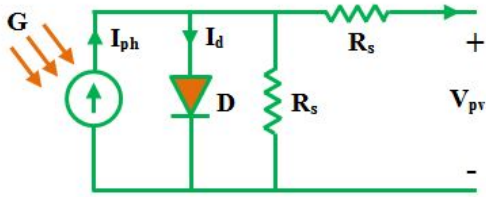


Fig. 1. Equivalent Circuit of Solar Photovoltaic (SPV) Cell.

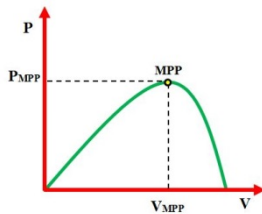


Fig. 2. PV Characteristics of SPV.

The accuracy of electrical parameters in SPV cells can be known by I - V and P - V curves which offer the data for the design, installation and maintenance of SPV systems. Fig. 2 shows P - V characteristics of SPV system. The specification considered for the SPV panel is given in Table 1.

Table 1. Specification for SPV Panel

Parameter	Specification
Number of cells in series	ncells = 72
Maximal power, W	$P_{max} = 320 \text{ W}$
Maximal power voltage, V	$V_{max} = 37.1 \text{ V}$
Maximal power current, A	$I_{max} = 8.62 \text{ A}$
Voltage in open circuit, V	$V_{oc} = 45 \text{ V}$
Current in short circuit, A	$I_{sc} = 9.08 \text{ A}$

The incorporation of the SPV system has SPV cells in modules; VSI and AC filter which are connected to the main grid. Fig. 3 shows the simple layout diagram of the SPV system which operates under the proposed e-ANOVA tuned controller in d - q control strategies. The SPV system supplies the load demand to maintain a constant power supply at variable loading conditions.

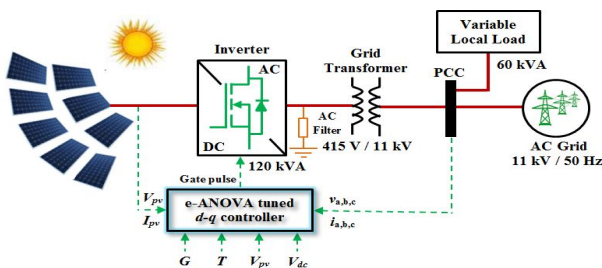


Fig. 3. An Incorporation of SPV System.

3. Implementation of Proposed SPV System

3.1 Brainwave to ANOVA Techniques

ANOVA theory and its applications were developed by Professor R. A. Fisher. In fact, he used the term ‘Variance’ first, later Professor Snedecor and many researchers came up with the development of these techniques. The ANOVA techniques are used for optimization in several fields like economics, psychology, sociology, etc. The proposed e-ANOVA method is used for PI in d - q controller with the effects of the optimal gate pulse for VSI and is grabbed by the intended techniques of ANOVA. Fig. 4 shows the flowchart of ANOVA techniques.

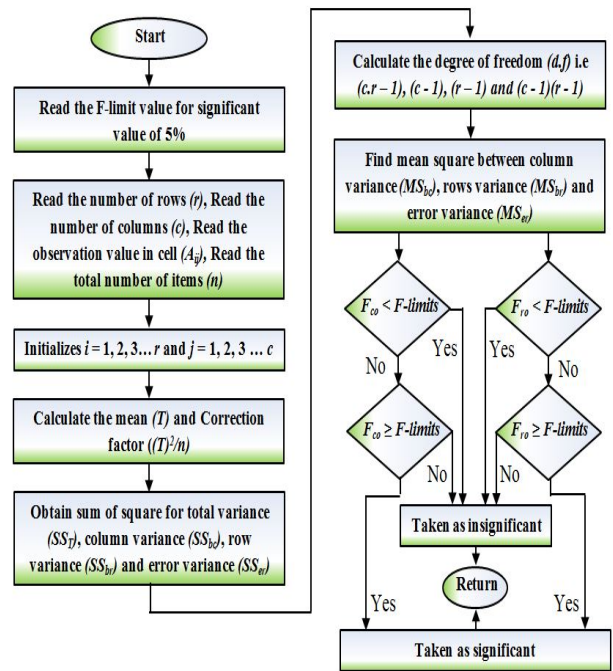


Fig. 4. Flowchart for ANOVA Techniques.

An ANOVA method is introduced in this research work for the PI in d - q controller to yield more power from the SPV system. Before starting this ANOVA method, the following assumptions are made.

- A normal population is drawn from each of the samples.
- The same variance is assumed for each of these populations.
- All the factors being tested are effectively controlled.

3.2 Belief of ANOVA Methods

In the biological research process, the ANOVA methods were proposed as an optimization solution with ‘population’ at the initial set of the variable which concludes by the value of the F -table. The optimal ANOVA method practice certain forms of statistical hypothesis tests by comparing the calculated value of F -ratio to the F -limit value for the conclusion of either alternative hypothesis (H_A) or null hypothesis (H_0).

To determine this difference in the factor two-way or double-factor ANOVA method had been chosen. The 5% significant value is chosen for *F-limit*.

$$\left. \begin{aligned} H_0 : \mu_i = \mu \quad \text{all } i = 1,2,3 \dots r \\ H_A : \mu_i \neq \mu \quad \text{some } i = 1,2,3 \dots r \end{aligned} \right\} \quad (5)$$

$$\left. \begin{aligned} H_0 : \mu_i = \mu \quad \text{all } i = 1,2,3 \dots c \\ H_A : \mu_i \neq \mu \quad \text{some } i = 1,2,3 \dots c \end{aligned} \right\} \quad (6)$$

Step 1: For each sample, calculate the mean *i.e*

$$\text{Calculate } T = \sigma(A_{i,j}) \quad (7)$$

if, $i = 1, 2, 3 \dots r ; j = 1, 2, 3 \dots c$

Where, ‘*i*’ is the row factor, ‘*j*’ is the column factor,

‘*r*’ is number of row factor, ‘*c*’ is number of column factor

‘*A_{ij}*’ is the observation value given in (*ij*)th cell

Step 2: Calculate the correction factor *i.e* correction factor = $\frac{(T)^2}{n}$ (8)

Where, ‘*n*’ is the total number of items in (*ij*)th cell

Step 3: Obtain the sum of squares for total variance

$$\text{Total SS } (SS_T) = \sigma(A_{i,j})^2 - \frac{(T)^2}{n} \quad (9)$$

Where, $i = 1, 2, 3 \dots ; j = 1, 2, 3 \dots$

Step 4: Obtain the sum of squares for variance between column samples

$$\text{SS between column } (SS_{bc}) = \sigma\left(\frac{(T_j)^2}{n_j}\right) - \frac{(T)^2}{n} \quad (10)$$

Where, $j = 1, 2, 3 \dots c$

Step 5: Obtain the sum of squares for variance between row samples

$$\text{SS between column } (SS_{br}) = \sigma\left(\frac{(T_i)^2}{n_i}\right) - \frac{(T)^2}{n} \quad (11)$$

Where, $i = 1, 2, 3 \dots r$

Step 6: Find the sum of squares of deviations for error variance

$$\text{SS for error variance } (SS_{er}) = (SS_T) - (SS_{bc} + SS_{br}) \quad (12)$$

Step 7: Degrees of freedoms (*d.f*) can be given by

$$\left. \begin{aligned} SS_T &= (c.r - 1) \\ SS_{bc} &= (c - 1) \\ SS_{br} &= (r - 1) \\ SS_{er} &= (c - 1)(r - 1) \end{aligned} \right\} \quad (13)$$

Step 8: Calculate the ratio of the sum of squares for variance between column samples to the degree of freedom (*d.f*) *i.e* (*c - 1*).

$$\text{Mean square between columns } (MS_{bc}) = \frac{(SS_{bc})}{(c - 1)} \quad (14)$$

Step 9: Calculate the ratio of the sum of squares for variance between row samples to the degree of freedom (*d.f*) *i.e* (*r - 1*).

$$\text{Mean square between rows } (MS_{br}) = \frac{(SS_{br})}{(r - 1)} \quad (15)$$

Step 10: Calculate the ratio of the sum of squares of deviation for error variance to the degree of freedom (*d.f*) *i.e* (*c - 1*) (*r - 1*)

$$\text{Mean square for error variance } (MS_{er}) = \frac{(SS_{er})}{(c - 1)(r - 1)} \quad (16)$$

Step 11: Calculate the *F-ratio* between columns can be given as

$$F - \text{ratio in columns } (F_{co}) = \frac{(MS_{bc})}{(MS_{er})} \quad (17)$$

Step 12: Calculate the *F-ratio* between rows can be given as

$$F - \text{ratio in rows } (F_{ro}) = \frac{(MS_{br})}{(MS_{er})} \quad (18)$$

The various steps of ANOVA methods can be summarised as shown in Table 2.

3.3 Implementation of ANOVA Methods

The practice of ANOVA is employed with statistical methods which are practically implemented by the researchers to regulate the optimal condition in order to obtain the value of the desired outcome. The statistical method of ANOVA is a collective sample of a population that is related to foreseen procedures that are used to analyse the variances among group means in a sample. Basically, the ANOVA method is used to estimate a continuous response through different levels of a factor. An ANOVA method is employed under the assumption that the procedures are undergoing investigation of Gaussian noise with normal distribution.

In this research, two-way ANOVA methods are preferred for tuning the PI in the *d-q* controller for the purpose of optimum value of proportional gain (*K_p*) and integral gain (*K_i*). By the way of priori test, the statistical population represented by the data sets is chosen for sample groups by means of the population.

Table 2. Summarised Steps of ANOVA Methods

Source of Variation	Sum of Squares (SS)	Degree of freedom (<i>df</i>)	Mean Square (MS)	<i>F</i> -ratio (Calculated Value of <i>F</i>)
Between Columns	SS_{bc}	$(c - 1)$	$\frac{SS_{bc}}{(c - 1)}$	$F_{co} = \frac{MS_{bc}}{MS_{er}}$
Between Rows	SS_{br}	$(r - 1)$	$\frac{SS_{br}}{(r - 1)}$	$F_{ro} = \frac{MS_{br}}{MS_{er}}$
Error	SS_{er}	$(c - 1)(r - 1)$	$\frac{SS_{er}}{(c - 1)(r - 1)}$	
Total	$\sigma(A_{ij})^2 - \frac{(T)^2}{n}$	$(c.r - 1)$		

The two sets of data taken from observation and arranged in rows and columns form a group of samples. Each set forms the group data for K_p and K_i values of the controller. With the two-way ANOVA method, the mean of a sample and mean of a sample mean are obtained to estimate the sum of a square and mean square variance between columns, rows, and error of the samples as shown in Table 2. To reduce the training data time of the sample we represent the scaling factor equation as our research modification in equation (19) known as an e-ANOVA.

$$M'_{ij} = \frac{A_{ij} - \wedge(A_{ij})}{\vee(A_{ij}) - \wedge(A_{ij})} \quad (19)$$

From the observation of the ANOVA method is given by the generalized equation

$$A_{ij} - \mu_{ij} = \varepsilon_{ij} \sim N(0, \sigma^2) \quad (20)$$

Where, $\wedge(A_{ij})$ – is maximum observation

$\vee(A_{ij})$ – is minimum observation

A_{ij} – is the observation value given in $(ij)^{th}$ cell

μ_{ij} – is overall mean given in $(ij)^{th}$ cell

ε_{ij} – is error given $(ij)^{th}$ cell

Finally, the F_{co} value and F_{ro} value are compared with the *F*-limits value for the degree of freedom, to identify the best value of K_p and K_i is achieved. The proposed method reduces the complexity while depending on the sampling number of the population. The ANOVA methods control the overall Type I error rate *i.e* false-positive finding. It also holds true for the normality assumptions. The proposed e-

ANOVA tuned PI in *d-q* controller methods regulate the SPV power and inject the power to the grid with less distortion under the fast varying atmospheric condition. Also, it has the following advantages, 1) has higher perfection than the traditional methods, 2) reduces the training data time, 3) decreases the size of the input sample group and 4) retains the sample discretionary information.

4. Configuration of SPV System and its Operations

4.1 SPV Configuration

Fig. 3 shows the incorporation of the SPV system in single-stage power conversion. In general SPV system includes SPV array cells, VSI, and AC filters interconnect to the main grid.

4.2 ANOVA Tuned PI in *d-q* Controller

In this section, an ANOVA technique is adopted to extend the usefulness of an optimal design of PI controllers used in *d-q* control strategies. The *d-q* controller consists of four PI controllers as shown in Fig. 5. In this *d-q* controller two loops are framed which are named as current control loop and voltage control loop. Both the loops require the desired gain value of the PI controller determined by e-ANOVA techniques as an optimal gain of K_p and K_i is shown in Table 3. The current control loop permits the specific power to the grid, whereas the voltage control loop requires the predetermined reference voltage acceptable for supply to the domestic load.

From the point of coupling, the three-phase voltage and current are sensed and transformed to the corresponding *d-q* component by using Clarke’s transformation and Park’s transformation. In the voltage control loop, the summation of dc-link voltage (V_{dc}), and the reference dc-link voltage (V_{dref}) gives up the error which flows through the PI controller. The outturn of PI controller offers the current

controller (i'_d) of d -axis and is compared with real grid current (i_d) of d -axis for the dc-link voltage control.

Table 3. PI Controllers Gains

Parameter	Proportional Gain (K_p)	Integral Gain (K_i)
Current Control Loop	0.924	283
Voltage Control Loop	0.985	252

At the same time, the q -axis component can be compared with reference bus voltage (V_{busref}) and grid voltage (V_{bus}) similar to d -axis, but in this case, it has zero effect on the q -axis [25].

In the current control loop [26, 27], the voltage reference value is obtained from the SPV system as $-v^*_d$ and $-v^*_q$ which are elevated along with grid voltage value as new d - q voltage value given by equations (21) and (22).

$$V_{dnew} = R(i_d) + L \frac{d(i_d)}{dt} - \omega L(i_q) + v_\alpha \quad (21)$$

$$V_{qnew} = R(i_q) + L \frac{d(i_q)}{dt} - \omega L(i_d) + v_\beta \quad (22)$$

Finally, the new d - q voltage is transformed to three-phase voltage and current by using Inverse Park transformation. The phase-locked loop (PLL) tracks the

changes in the phase of the grid and maintains the theta value of both the frequency of the grid and the SPV system. In the end, the output of Inverse Park transformation *i.e* three-phase abc voltage (V_{abcl}) is equated to the PWM modulator to generate the gate pulses for VSI.

5. Simulation Results and its Discussion

5.1 Proposed SPV Model

The SPV system has been chosen with 5 SPV modules as a string of 37.1 V per module and the string voltage of 185.5 V as a SPV voltage (V_{pv}). The proposed SPV system consists of SPV array cells, VSI, and AC filters which interconnect to the main grid. The proposed SPV system manages the inflexible voltage; by reforming the optimized gate pulse of the inverter in order to achieve the optimal power of the SPV system. An elaborate difference is given in this section to express a common analysis for a probability to pick out the proposed ANOVA tuned d - q controller in the SPV system. A complete analysis is done by MATLAB/Simulink to extract non-linear time-domain specifications. Through this section, relative learning has been carried out between the proposed systems as e-ANOVA tuned PI in d - q controller with conventional systems as d - q controller. The simulation parameter chosen for SPV system configuration is given in the Table 4.

5.2 Performance Analysis of SPV Model

The SPV system analysis is tested under steady-state, dynamic state and grid performance by choosing constant temperature 25°C with uniform irradiance and variable irradiance. In this study the current of proposed and conventional system is assumed to be constant.

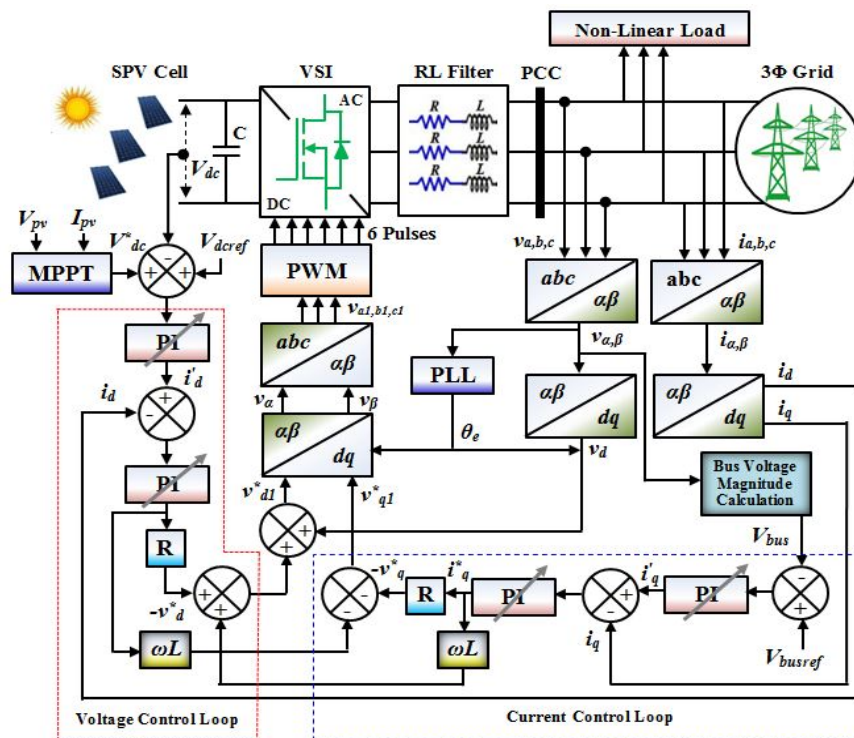


Fig. 5. Proposed e-ANOVA Tuned PI d - q Controller for VSI

Table 4. SPV System Configuration Parameters Chosen for the Simulation

SPV description	Parameters	Ratings
AC Grid	Line voltage / frequency	11 kV / 50 Hz
VSI	Capacity / Voltage	120 kVA / 415 ± 1% V
Grid transformer	Voltage rating	415 V/11 kV
PV system	SPV description	Refer the Table 1
Variable local load	Unbalanced load	60 kVA, lagging

5.3 Behaviour of system in steady-state at uniform irradiance

The steady-state analysis is achieved for uniform irradiance of 1000 W/m² as shown in Fig. 6(a) and Fig. 6(b) illustrates the PV array voltage of proposed and conventional systems. The effects of the proposed and the conventional systems are indicated in Fig. 6(c) shows the SPV array power.

The proposed method shows an enhancement in terms of response time in 0.117 s but the conventional controller as 0.883 s. Further, an illustration shows that the SPV output power is settled within 0.11 s and 0.88 s for intended and conventional controllers respectively.

The overshoot percentage of the proposed controller is 28.72% whereas the conventional controller is 45.34%. Table 5 shows the summary of the steady-state analysis of with and without ANOVA tuned controller. The peak power is closely 146.73 W and 164.47 W for the proposed and conventional controllers respectively. Summary of Table 5 and the simulation illustrations point out that the proposed controller affords suitable results in the stability for the uniform irradiance. Also, the e-ANOVA tuned *d-q* controller shows good performance in the steady-state analysis than the conventional controller.

5.4 Behaviour of System in Dynamic State at Variable Irradiance

The dynamic analysis is attained for variable irradiance from 500 W/m² to 900 W/m² as shown in Fig. 7(a). This analysis is examined in two cases (i) increase in irradiance (with 50 W/m², 100 W/m², and 200 W/m²) and (ii) decrease in irradiance (with 100 W/m², 150 W/m², and 200 W/m²). Fig. 7(b) illustrates the PV array voltage of proposed and conventional systems. The outcomes of the intended and the conventional systems illustrated in Fig. 7(c) shows the SPV array power.

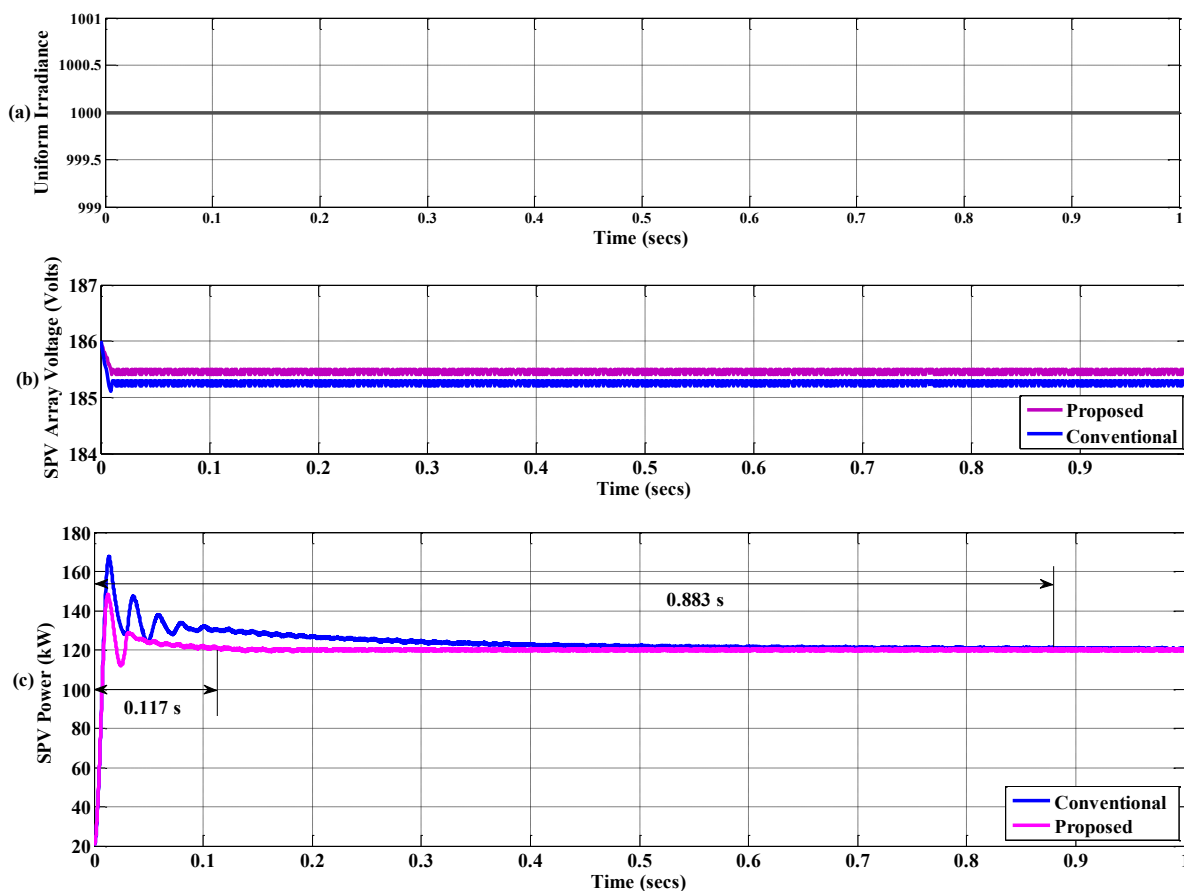


Fig. 6. Performance of SPV System under Steady State Analysis (a) Uniform Irradiance at 1000 W/m² (b) SPV Array Voltage in volts (c) SPV Power Generation in kW.

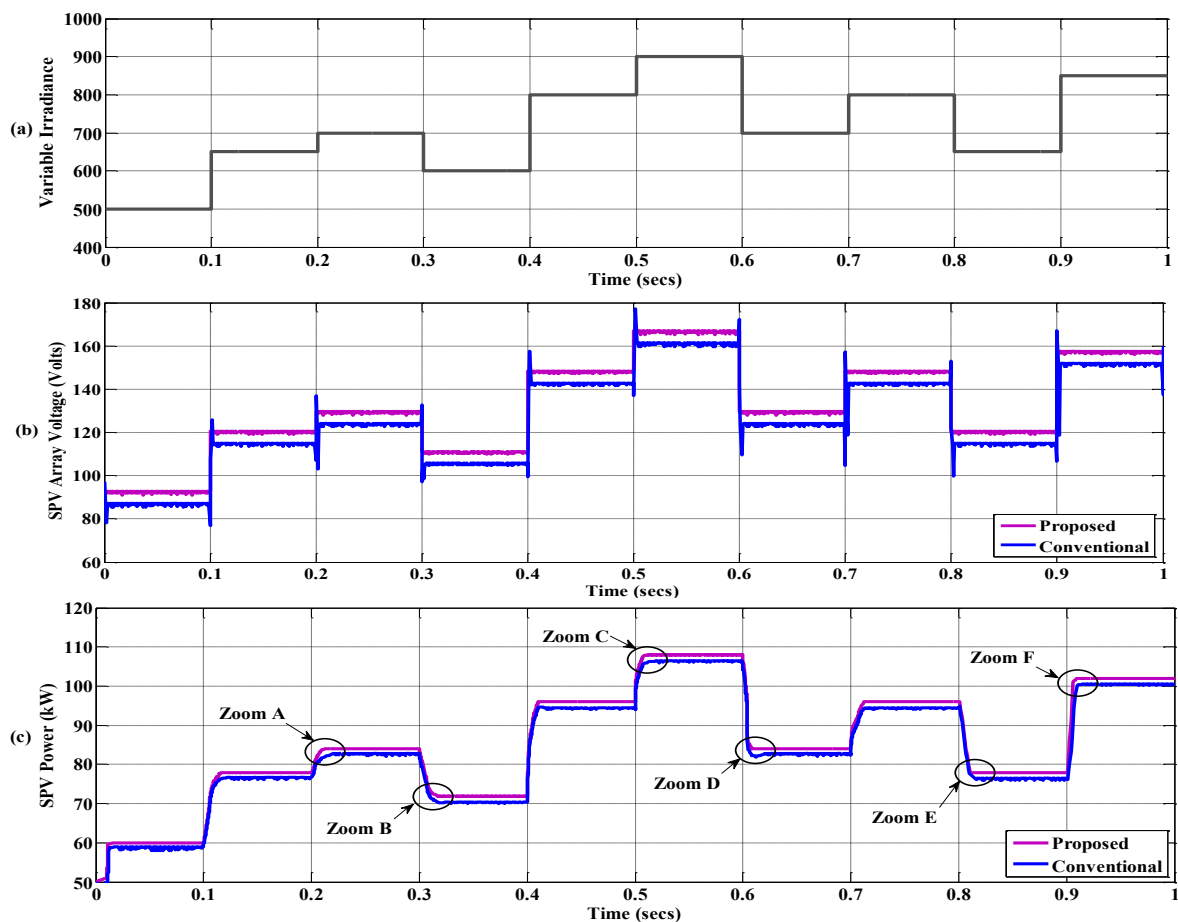


Fig. 7. Performance of SPV System under Dynamic State (a) Variable Irradiance 500 W/m² to 900 W/m² (b) SPV Array Voltage in volts (c) SPV Power Generation in kW.

Table 5. Steady State under Uniform Irradiance

Factors	Without ANOVA (Conventional Controller)	With ANOVA (Proposed Controller)
Rise time (s)	0.019	0.017
Peak time (s)	0.026	0.021
Settling time (s)	0.883	0.117
Overshoot (%)	45.34	28.72
Settling Min Power (kW)	117.89	119.95
Settling Max Power (kW)	145.65	128.38
Peak Power (kW)	164.47	146.73

5.5 Performance of Dynamic State at Increase in Irradiance

The dynamic performance of the proposed and the conventional system is indicated in Fig. 7(c) as zoom view of Zoom A, Zoom C, Zoom F with 50 W/m², 100 W/m², 200 W/m² increase in irradiance respectively as shown in Fig. 8(a)(b)(c). Table 6 shows the quick summary of the dynamic performance of both proposed and conventional controllers for increase in irradiance.

5.6 Performance of Dynamic State at Decrease in Irradiance

The dynamic performance of the proposed and the conventional system is indicated in Fig. 7(c) as zoom view of Zoom B, Zoom D, Zoom E with 100 W/m², 200 W/m², 150 W/m² decrease in irradiance respectively as shown in Fig. 9(a)(b)(c). Table 7 shows the quick summary of the dynamic performance of both proposed and conventional controller for decrease irradiance. Also, the proposed controller shows a better performance in dynamic analysis when compared to the conventional controller. Additionally, the proposed ANOVA tuned *d-q* controller shows an improvement in terms of response time relative to the period of fast varying environment conditions against the conventional *d-q* controller.

5.7 Behaviour of SPV System in Grid

The performance analysis of the SPV system in the grid is considered by changes in irradiation and variable load conditions.

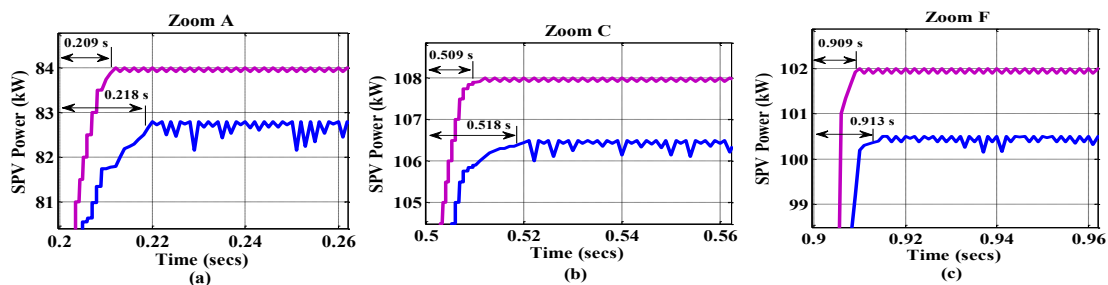


Fig. 8. Zoomed view of Grid power in kW (a) Zoom A increase in the irradiance of 50 W/m² (b) Zoom C increase in the irradiance of 100 W/m² (c) Zoom F increase in the irradiance of 200 W/m².

Table 6. Dynamic Analysis for Variable Increase Irradiance

Factors	Without ANOVA (Conventional Controller)			With ANOVA (Proposed Controller)		
	Point A	Point C	Point F	Point A	Point C	Point F
Rise time (s)	0.218	0.518	0.913	0.209	0.509	0.909
Peak time (s)	0.220	0.521	0.915	0.211	0.512	0.910
Settling time (s)	0.223	0.523	0.919	0.213	0.513	0.910
Overshoot (%)	65.13	51.48	43.23	09.12	11.16	10.12
Settling Min Power (kW)	82.15	106.1	101.91	83.91	107.9	101.91
Settling Max Power (kW)	82.80	106.5	100.50	84.00	108.0	102.00
Peak Power (kW)	82.85	106.5	100.53	84.01	108.0	102.02

Table 7. Dynamic Analysis for Variable Decrease Irradiance

Factors	Without ANOVA (Conventional Controller)			With ANOVA (Proposed Controller)		
	Point B	Point D	Point E	Point A	Point D	Point E
Rise time (s)	0.319	0.612	0.815	0.316	0.608	0.811
Peak time (s)	0.320	0.614	0.816	0.318	0.609	0.812
Settling time (s)	0.326	0.619	0.818	0.319	0.610	0.813
Overshoot (%)	46.25	62.32	50.15	12.02	05.12	13.38
Settling Min Power (kW)	70.10	82.15	77.88	71.88	83.95	77.88
Settling Max Power (kW)	70.55	82.83	76.50	72.01	84.00	78.00
Peak Power (kW)	70.00	82.80	76.15	72.00	84.01	78.02

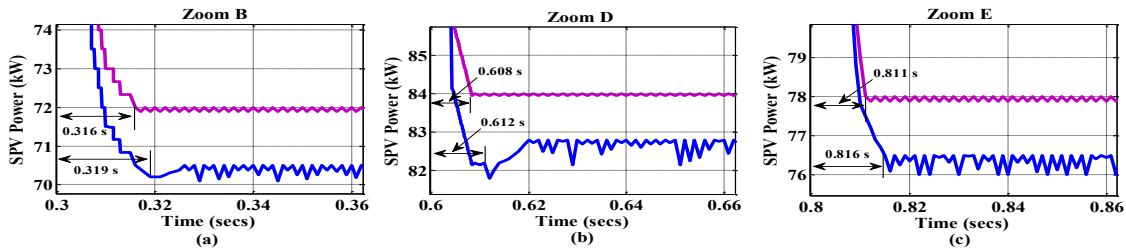


Fig. 9. Zoomed view of Grid power in kW (a) Zoom B decrease in the irradiance of 100 W/m² (b) Zoom D decrease in the irradiance of 200 W/m² (c) Zoom E decrease in the irradiance of 150 W/m².

Also, the SPV power injected from inverter to grid and the load is examined by harmonic distortion for both proposed and conventional systems. The conventional grid voltage and the current waveform is shown in Fig. 10, twist out of shape due to the connection of nonlinear load at PCC. The total harmonic distortion of conventional grid voltage 0.10% and a current 6.79% are above the limitation of harmonic content imposed by international standards as shown in Fig. 11.

The proposed grid voltage and current are shown in Fig. 12 which is less distorted than the conventional system. Fig. 13 shows the total harmonic distortions which lie under the limitation of harmonic content imposed by international standards. The THDs value of the proposed grid voltage is 0.09% and the current is 2.17%. Hence, the grid performance of the proposed e-ANOVA tuned *d-q* controller for the SPV system is preferable to the conventional *d-q* controller.

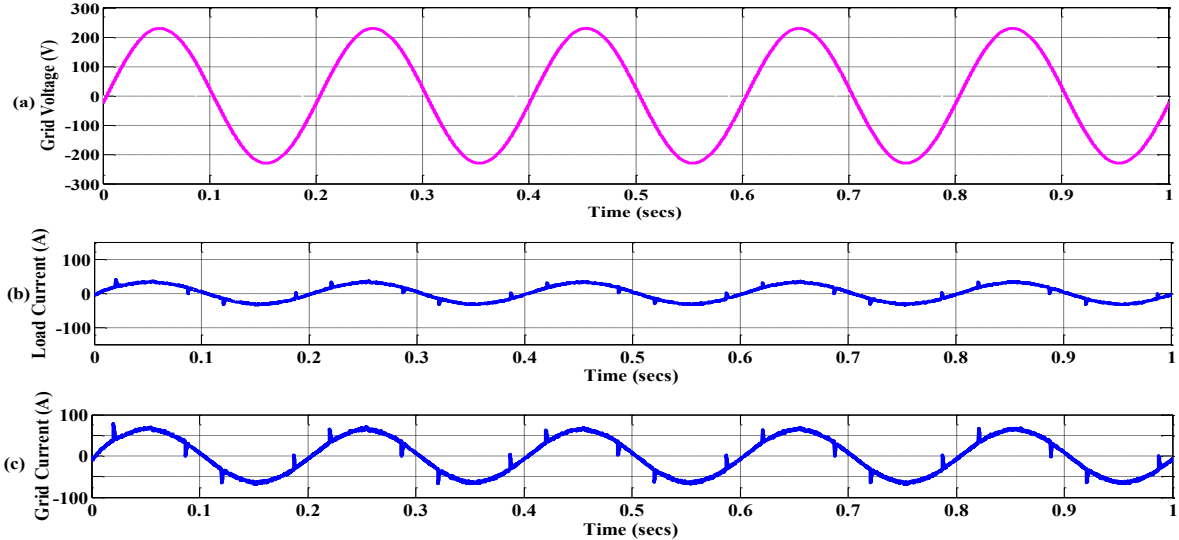


Fig. 10. Grid Performance of Conventional System (a) Grid Voltage in per phase (b) Load Current in per phase (c) Grid Current in per phase.

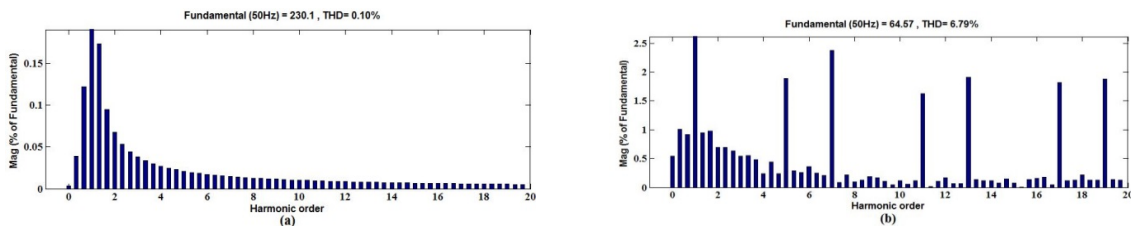
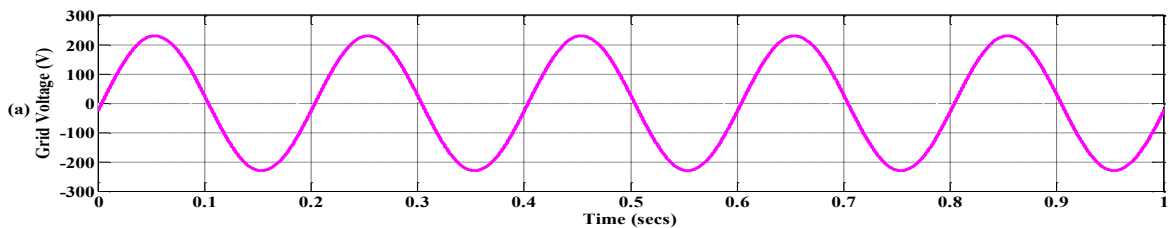


Fig. 11. FFT Analysis of Conventional System (a) Voltage THDs and (b) Currents THDs.



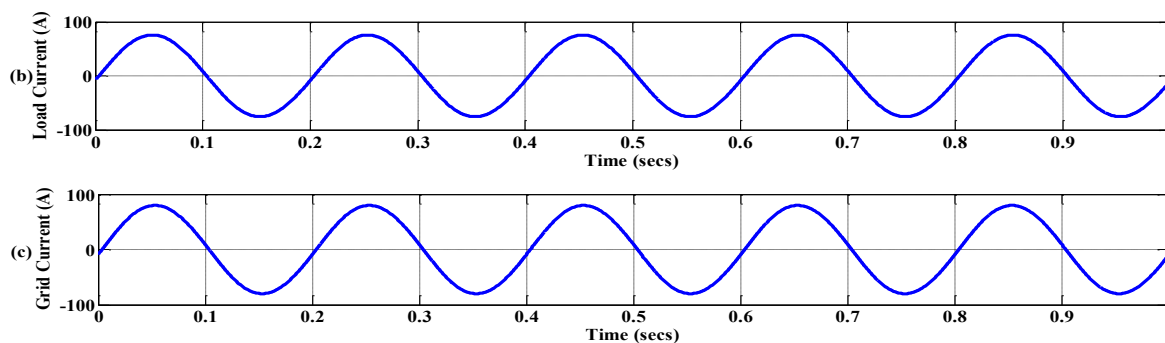


Fig. 12. Grid Performance of Proposed System (a) Grid Voltage in per phase (b) Load Current in per phase (c) Grid Current in per phase.

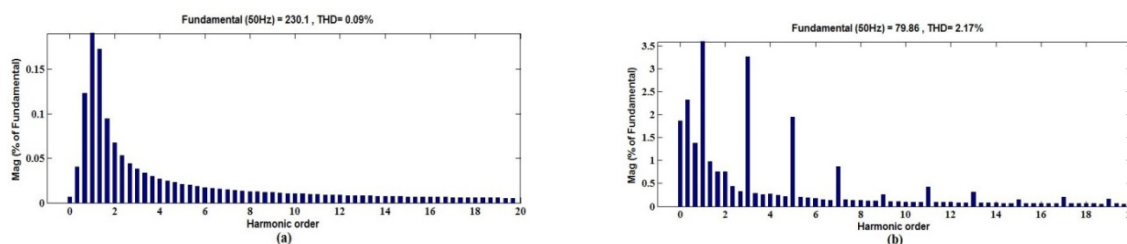


Fig. 13. FFT Analysis of Proposed System (a) Voltage THDs and (b) Currents THDs.

6. Conclusion

An e-ANOVA tuned $d-q$ controller has been demonstrated for a three-phase single-stage grid integrated SPV system. The purports of e-ANOVA tuned $d-q$ controller approach reforms the grid performance and power quality. The performance of e-ANOVA tuned $d-q$ controller is examined under steady-state and dynamic state conditions. During the uniform irradiance conditions, the e-ANOVA tuned $d-q$ controller alone determines the optimal power of the SPV system and also in the variable irradiance conditions. The comparative analysis of the time-domain specification of amplitude extracting performance of SPV power has effectively demonstrated for the conventional and proposed system. The proposed response time of SPV power 146.73 kW is 0.117 s, whereas for power 164.47 kW is 0.883 s for the conventional system at uniform irradiance. Similarly, variable irradiance of the proposed response time of SPV power 84.01 kW, 108 kW, and 102.02 kW is 0.208 s, 0.509 s, and 0.908 s respectively whereas for conventional power 82.85 kW, 106.5 kW, and 100.53 kW are 0.217 s, 0.518 s, and 0.913 s respectively for the increase in the irradiance, and the proposed response time of SPV power 72 kW, 84.01 kW, and 78.02 kW are 0.316 s, 0.608 s, and 0.811 s respectively whereas conventional power 70.02 kW, 82.80 kW, and 76.15 kW are 0.319 s, 0.612 s, and 0.815 s respectively for the decrease in the irradiance. The grid performance in terms of THDs for voltage is 0.10% and current is 6.79% for the proposed system whereas in conventional voltage is 0.09% and current is 2.17%. The THDs of the intended system achieved the grid code limitations of international standards. The simulation was implemented in MATLAB/Simulink environment and the results were observed that the proposed e-ANOVA tuned $d-q$ controller reforms the grid performance and power quality in the SPV system.

References

- [1] L. Zhang, S. Shenglong Yu, T. Fernando, H. Ho-Ching Iu, K. Po Wong, "An online maximum power point capturing technique for high-efficiency power generation of solar photovoltaic systems". *J Mod Power Syst Clean Energy*, <https://doi.org/10.1007/s40565-018-0440-2>, Vol 7: pp. 357–368, 2019.
- [2] J. C. Schaefer, "Review of photovoltaic power plant performance and economics", *IEEE Trans Energy Convers*, <https://doi.org/10.1109/60.107215>, Vol 5:232–238, 1990.
- [3] M. Al-Dhaifallah, A. M. Nassef, H. Rezk, K. Soopy Nisar, "Optimal parameter design of fractional order control based INC-MPPT for PV system" *Sol Energy*, <https://doi.org/10.1016/j.solener.2017.11.040>, Vol 159:650–664, 2018.
- [4] A. Elmelegi, M. Aly, E. M. Ahmed, A. G. Alharbi, "A simplified phase-shift PWM-based feed forward distributed MPPT method for grid-connected cascaded PV inverters", *Sol Energy*, <https://doi.org/10.1016/j.solener.2019.05.021>, Vol 187:1–12, 2019.
- [5] M. Abdel-Salam, M-T. EL-Mohandes, M. Goda, *History of Maximum Power Point Tracking*. In: A. M. Eltamaly, A. Y. Abdelaziz (eds) *Modern Maximum Power Point Tracking Techniques for Photovoltaic Energy Systems*. Springer International Publishing, Ch, pp 1–29
- [6] B. Pakkiraiah, G. Durga Sukumar, "Research Survey on Various MPPT Performance Issues to Improve the Solar PV System Efficiency", *J. Sol. Energy*, Jun 2016.
- [7] R. López-Erauskin, A. González, G. Petrone, G. Spagnuolo, J. Gyselinck, "Multi-Variable Perturb and

- Observe Algorithm for Grid-Tied PV Systems With Joint Central and Distributed MPPT Configuration”. *IEEE Trans Sustain Energy*, Vol 12 PP. 360 – 367, 2021.
- [8] M. Alsumiri, “Residual Incremental Conductance Based Nonparametric MPPT Control for Solar Photovoltaic Energy Conversion System”. *IEEE Access*, <https://doi.org/10.1109/ACCESS.2019.2925687>, Vol 7, pp. 87901–87906, 2019.
- [9] T. Sen, N. Pragallapati, V. Agarwal, R. Kumar, “Global maximum power point tracking of PV arrays under partial shading conditions using a modified particle velocity-based PSO technique”, *IET Renew Power Gener*, <https://doi.org/10.1049/iet-rpg.2016.0838>, Vol 12, pp. 555–564, 2018.
- [10] H. Li, D. Yang, W. Su, J. Lü, X. Yu, “An Overall Distribution Particle Swarm Optimization MPPT Algorithm for Photovoltaic System Under Partial Shading”, *IEEE Trans Ind Electron*, <https://doi.org/10.1109/TIE.2018.2829668>, Vol 66 pp. 265–275, 2019.
- [11] A. Nouri, I. Salhi, E. Elwarraki, S. El Beid, N. Essounbouli, “DSP-based implementation of a self-tuning fuzzy controller for three-level boost converter”, *Electr Power Syst Res*, <https://doi.org/10.1016/j.epsr.2017.01.036>, Vol 146, pp. 286–297, 2017.
- [12] G. Bayrak, D. Ghaderi, “An improved step-up converter with a developed real-time fuzzy-based MPPT controller for PV-based residential applications”, *Int Trans Electr Energy Syst*, <https://doi.org/10.1002/2050-7038.12140>, Vol 29, pp. e12140, 2019.
- [13] K. Okedu, A. S. AlSenaidi, I. A. Rashdi, and W. A. Salmani, “Real Time Dynamic Analysis of Solar PV Integration for Energy Optimization,” *Int. J. Smart Grid-IJSmartGrid*, Vol. 4, no. 2, Art. No. 2, Jun 2020.
- [14] S. Ozdemir, N. Altin, I. Sefa, “Single stage three level grid interactive MPPT inverter for PV systems”, *Energy Convers Manag*, <https://doi.org/10.1016/j.enconman.2014.01.048>, Vol 80, pp. 561–572. 2014.
- [15] F. Ayadi, I. Colak, I. Garip, and H. I. Bulbul, “Impacts of Renewable Energy Resources in Smart Grid,” in *2020 8th International Conference on Smart Grid (icSmartGrid)*, Jun. 2020, pp. 183–188. doi: 10.1109/icSmartGrid49881.2020.9144695.
- [16] D. Siswantoro and S. L. Z. Ridho, “Is Grid Solar Power Still Attractive Amid Decreasing Fuel Prices? The Case of Indonesian Electrical Power,” *Int. J. Smart Grid - IJSmartGrid*, vol. 5, no. 2, Art. no. 2, Jun. 2021.
- [17] R. S. Muñoz-Aguilar, I. Candela, J. Rocabert, and P. Rodríguez, “Grid resonance attenuation in long lines by using renewable energy sources,” in *2017 IEEE 6th International Conference on Renewable Energy Research and Applications (ICRERA)*, Nov. 2017, pp. 429–434. doi: 10.1109/ICRERA.2017.8191098.
- [18] S. F. Jaber and A. M. Shakir, “Design and Simulation of a Boost-Microinverter for Optimized Photovoltaic System Performance,” *Int. J. Smart Grid - IJSmartGrid*, Vol. 5, no. 2, Art. no. 2, Jun. 2021
- [19] G. Bayrak, D. Ghaderi, U. Subramaniam, “Leakage current repression and real-time spectrum analysis with chirp Z-transform for a novel high-efficiency PV-based inverter applicable in micro-grids”, *Electr Eng*, <https://doi.org/10.1007/s00202-020-01002-w>, Vol 102, pp. 2041–2057, 2020.
- [20] J. Wang, X. Liu, Y. Xun, S. Yu, “Common Mode Noise Reduction of Three-Level Active Neutral Point Clamped Inverters With Uncertain Parasitic Capacitance of Photovoltaic Panels”, *IEEE Trans Power Electron*, <https://doi.org/10.1109/TPEL.2019.2956771>, Vol 35, pp. 6974–6988, 2020.
- [21] Y. Geng, K. Yang, Z. Lai, P. Zheng, H. Liu, R. Deng, “A Novel Low Voltage Ride Through Control Method for Current Source Grid-Connected Photovoltaic Inverters”, *IEEE Access*, <https://doi.org/10.1109/ACCESS.2019.2911477>, Vol 7, pp. 51735–51748, 2019.
- [22] A. Belkaid, I. Colak, K. Kayisli, and R. Bayindir, “Improving PV System Performance using High Efficiency Fuzzy Logic Control,” in *2020 8th International Conference on Smart Grid (icSmartGrid)*, Jun. 2020, pp. 152–156. doi: 10.1109/icSmartGrid49881.2020.9144817.
- [23] N. Pachaivannan, R. Subburam, U. Ramkumar, P. Kasinathan, “Crowded plant height optimisation algorithm tuned maximum power point tracking for grid integrated solar power conditioning system”, *IET Renew Power Gener*, <https://doi.org/10.1049/iet-rpg.2018.5053>, Vol 13, pp. 2137–2147, 2019.
- [24] N. Pachaivannan, R. Subburam, M. Padmanaban, A. Subramaniam, “Certain investigations of ANFIS assisted CPHO algorithm tuned MPPT controller for PV arrays under partial shading conditions”. *J Ambient Intell Humaniz Comput*. <https://doi.org/10.1007/s12652-020-02738-w>, January 2021.
- [25] S. Prakash, S. Purwar, S. R. Mohanty, “Adaptive Detection of Islanding and Power Quality Disturbances in a Grid-Integrated Photovoltaic System”, *Arab J Sci Eng*, <https://doi.org/10.1007/s13369-020-04378-w>, Vol 45, pp. 6297–6310, 2020.
- [26] A. Ahmad, L. Rajaji, A. Iqbal, “A novel current controller design for grid-integrated PV inverter system”, *SN Appl Sci*, <https://doi.org/10.1007/s42452-021-04290-4>, Vol 3, pp. 323, 2021.
- [27] A. Bouhouta, S. Moulahoum, N. Kabache, and I. Colak, “Simplicity and Performance of Direct Current Control DCC Compared with other Identification Algorithms for Shunt Active Power Filter,” in *2018 7th International Conference on Renewable Energy Research and Applications (ICRERA)*, Oct. 2018, pp. 1352–1357. doi: 10.1109/ICRERA.2018.8566973.